UNIVERSITÀ DEGLI STUDI DI PADOVA

Dipartimento di Fisica e Astronomia "Galileo Galilei"

Corso di Laurea in Fisica

Tesi di Laurea

Variazioni sul Freeze-Out di Materia Oscura

Variations on Dark Matter Freeze-Out

Relatore

Prof. Francesco D'Eramo

Laureando

Francesco Peroni

Anno Accademico 2023/2024

Riassunto

In questa tesi viene dapprima fornita una descrizione dei fenomeni gravitazionali che hanno portato all'ipotesi dell'esistenza della materia oscura. Successivamente, viene esaminato lo stato attuale delle conoscenze riguardanti la materia oscura, elencando i vincoli teorici e osservativi delle sue varie proprietà. Vengono poi considerati diversi modelli e candidati per la materia oscura, con particolare attenzione al modello delle WIMPs termiche, ovvero particelle massive debolmente interagenti in grado di annichilirsi tra loro, generando particelle del Modello Standard. Questa proprietà consente loro di rimanere in equilibrio termico e chimico con il plasma primordiale nelle prime fasi dell'universo. In base a questa ipotesi, viene studiato il processo di disaccoppiamento della materia oscura dal bagno termico primordiale, utilizzando il modello del freeze-out istantaneo e l'equazione di Boltzmann. Si dimostra che tale processo conduce alla stabilizzazione della densità di materia oscura nell'universo, mantenendola costante nel tempo.
Infine, viene esplorato l'effetto di un'eventuale risonanza nella sezione d'urto del processo di annichilazione menzionato, analizzando come la presenza di tale risonanza possa influenzare la densità attuale della materia oscura, introducendo un significativo effetto di soppressione.

Contents

Introduction

Dark Matter (DM) is a fundamental problem in modern physics. The presence of different gravitational phenomena, which exhibit behaviors differing from those predicted by the theory of General Relativity (GR), leads to two possibilities for fundamental physics: to hypothesize that GR is an approximation of a more general theory or to assume the presence of undetected matter to account for the observed behavior.

Given the countless tests that have validated GR with great precision and the issues faced by modified gravity theories (such as their inability to explain all problematic observations), the second option currently seems more probable.

Given this assumption, the choice still leaves the field broad, as numerous models of particles —and not just particles—have been developed to explain the presence of unobserved gravity- interacting matter.

In this thesis, we first provide strong observational evidences for the necessity of assuming the existence of Dark Matter. Secondly, we give a brief introduction to what is known about Dark Matter. Assuming the Weakly Interacting Massive Particles (WIMPs) model, we then proceed to derive the Boltzmann equation. Finally, we discuss the case where a pole is present in the annihilation cross-section.

Chapter 1

Evidences and Constraints of Dark Matter

The aim of this chapter is to contextualize the framework within which Dark Matter is situated and within which we are working. In the first section, we provide a description of the observations that led to the formulation of the existence of Dark Matter and offer a historical review of its studies. In the second section, we gather information on what is currently known about Dark Matter, listing the constraints on its various properties.

1.1 Gravitation evidences for Dark Matter

The idea of the existence of dark, undetected material in our universe has been present since the beginning of science.
In 1844, the mathematician Friedrich Bessel predicted a companion star for Sirius and Procyon, respectively, to explain their observed motion.
In 1846, to explain the motion of Uranus, the French astronomer Urbain Le Verrier and the English astronomer John Couch Adams predicted the existence of a new planet, Neptune, which was discovered a few months later by Johann Galle.
Besides dark planets and dark stars, astronomers also discussed the existence of dark clouds, or dark "nebulae." By the end of the 19th century, the astronomical community was discussing large areas in the sky where there seemed to be many fewer stars. One of the first explanations for this was the presence of absorbing dark matter along the line of sight. This is regarded as one of the first examples of "dark matter" in the sky.
At the beginning of the 20th century, Lord Kelvin tried to determine the amount of dark matter in the Milky Way by applying gas theory to the stars. Although he did not exclude the possibility of dark matter, his calculations suggested that the fraction was negligible compared to visible matter. Similar calculations and conclusions were later made by Henri Poincaré and others. We can then conclude that in the first two decades of the 20th century, dark matter was regarded as indicative of faint stars, planets, and cold gas.
This perception started to change during the 1930s with the studies of Fritz Zwicky.

1.1.1 First Hints

Fritz Zwicky is one of the most famous pioneers in the field of dark matter, marking a turning point in its study. In 1933, he published an article in which he studied different galaxy clusters, using the redshift data published in 1931 by Edwin Hubble and Milton Humason.
In particular, in the Coma cluster, he noted a large scatter in the apparent velocities of eight galaxies, with differences of about 2000 km/s. This had previously been noted by Hubble and Humason, but Zwicky also tried to apply the Virial theorem to estimate the expected velocity dispersion of the galaxies in the cluster.

He obtained the total mass of the cluster by multiplying the number of observed galaxies, 800, by the average mass of a galaxy, which is about $10^9 M_\odot$ (data obtained from the study of Hubble and Humason). He also estimated the size of the cluster to be about 10^6 light-years. From this data, one can compute the velocity dispersion of the cluster.
We can do this explicitly. Using the Virial theorem for a gravitational potential, we have:

$$\langle T_{tot} \rangle = -\frac{1}{2} \langle V_{tot} \rangle \tag{1.1}$$

where $\langle T_{tot} \rangle$ is the kinetic energy and $\langle V_{tot} \rangle$ is the gravitational potential energy of the cluster, and the brackets indicate the average with respect to time.
We remark that the Virial theorem applies only to systems that are in equilibrium.
We can roughly estimate the potential energy of the clusters by assuming a uniform mass density distribution, yielding:

$$\langle V_{tot} \rangle = -\frac{3GM^2}{5R} \tag{1.2}$$

where M is the total mass of the cluster (approximately $10^{12} M_\odot$) and R is the radius of the cluster. To find $\sqrt{\langle v^2 \rangle}$, we compute:

$$\sqrt{\langle v^2 \rangle} = \sqrt{\frac{2T_{tot}}{M}} = \sqrt{\frac{V_{tot}}{M}} \tag{1.3}$$

This gives $\sqrt{\langle v^2 \rangle} \simeq 80$ km/s.
Although this is a rough computation, it yields a result consistent with Zwicky's findings. Note that the kinetic energy is measured relative to the frame at rest with respect to the galaxy cluster, so $\sqrt{\langle v^2 \rangle}$ represents the velocity dispersion of the system.
Observations indicate that the average velocity dispersion of galaxies is $\sqrt{\langle v^2 \rangle} \simeq 1000$ km/s. This strongly suggests that dark matter is significantly more prevalent than visible matter. At the time, Zwicky, like his predecessors, considered cold intergalactic gas as an explanation for his results.
Despite this, Zwicky's study is often regarded as the first strong observational evidence of dark matter. Interestingly, the term "dark matter," as previously noted, was already used within the astronomical community. It was not even the first instance of Zwicky using the term in a publication; he had used it earlier that year to describe the source of cosmic rays.
However, this study represents the first compelling evidence for a system predominantly composed of dark matter. In 1937, Zwicky published a follow-up article where he further refined his study of the Coma cluster. He revised the cluster's radius to about 2×10^7 light-years and estimated the presence of about 1000 galaxies. He also adjusted the velocity dispersion of the galaxies to 700 km/s. Based on this, he estimated the cluster's mass to be $4.5 \times 10^{10} M_\odot$.
Using direct observations and an estimate of the cluster's distance, he calculated an absolute luminosity of 8.5×10^7 times that of the Sun, which led to an unexpectedly high mass-to-light ratio of about 500. Note that Zwicky relied on Hubble's law (see A.1) for distance estimation, using a value of $H_0 = 558$ km/s/Mpc. We now know that $H_0 = 67.27 \pm 0.66$ km/s/Mpc, so Zwicky overestimated the light-to-mass ratio by about ten times. Nevertheless, this ratio remains high and indicates the presence of dark matter in some form. Meanwhile, in 1936, Sinclair Smith also derived a very high mass-per-galaxy value from his calculations on the Coma cluster.

During the 1950s and 1960s, further studies were conducted to explain the high mass-to-light ratios found by Zwicky and Smith. Initially, the applicability of the Virial theorem was debated. As mentioned earlier, the theorem is only valid for systems in equilibrium. Some astronomers, such as Erik Holmberg, suggested that the high velocities measured could be attributed to non-permanent members of the cluster.
This hypothesis was later dismissed, as it would imply that clusters were younger than the galaxies they contained. Meanwhile, astronomers began to investigate the composition of dark matter. Studies in the 1960s showed that neither cold nor hot gas could account for the missing mass.
More exotic possibilities, such as massive collapsed objects like dwarf stars or "snowballs," were also

explored. However, these possibilities were eventually ruled out by measurements of primordial light element abundances, supporting the idea that dark matter is non-baryonic. From now on, we will refer to Dark Matter with capital letters.
Nowadays to study the density profile of galaxy clusters, researchers exploit the hot gas within them. Assuming the gas is in hydrostatic equilibrium, the pressure of the gas is balanced by the gravitational pull:

$$\frac{dp(r)}{dr} = -\frac{G_N M(r)\rho(r)}{r^2} \tag{1.4}$$

Using the equation of state, we obtain the relationship between the pressure and the temperature of the gas:

$$p = \frac{\rho}{\mu m} T \tag{1.5}$$

From these relations, one can determine the mass distribution of the total mass once the radial density and temperature of the gas are measured. What is found is that, as it will be showed for galactic rotation curves, the visible mass is less than the total mass.

1.1.2 Galactic Rotation Curves

The understanding of galaxy rotation curves began to evolve in the 1970s with a more in-depth study of their characteristics.
It is important to note that these curves had been studied since the early 20th century, and through them, it was possible to determine the mass-to-light ratio of galaxies.
At that time, astronomers explained the observed excess mass by suggesting the presence of extinguished stars, dark clouds of gas, meteors, comets, and other debris. However, in 1970, Kent Ford and Vera Rubin studied the rotation curve of the Andromeda Galaxy (M31). For the first time, it became apparent that much more mass was needed to explain the observations, and that dark clouds of gas were insufficient. Later that same year, similar conclusions were drawn for other galaxies.
Throughout the 1970s, astronomers measured the velocity of stars in spiral galaxies as a function of their radial distance from the center and found that their rotation curves remained flat even at the largest observed optical radii, where the galaxy's matter is still detected through visible light. This was unexpected, as the velocities were anticipated to decrease. Later on, using radio telescopes and specifically the Doppler shift of the 21 cm hyperfine transition of neutral hydrogen, the same trend was observed at even larger radii.
We can easily understand why the rotation velocity curve was expected to drop rather than remain flat.
Assuming that standard Newtonian gravity is a good approximation for describing the motion of stars within galaxies, we would expect a star's circular velocity v_c around the galaxy's center to be:

$$v_c = \sqrt{\frac{GM}{r}} \tag{1.6}$$

Where M is the enclosed mass and r is the distance from the galactic center. If the star is on the periphery of the galaxy, then M, according to Gauss's law, is constant, and we would expect $v_c \propto 1/r^{1/2}$. However, it was found that the velocity distribution outside the galactic disk flattens, implying $M(r) \propto r$. This provided further evidences for the presence of matter around galaxies that is not visible to our telescopes, with a density profile very different from the mass distribution of visible matter.
The same conclusion would be reached even when accounting for the non-uniform mass distribution of spiral galaxies.
We conclude by noting that in 1963, Arrigo Finzi was the first to propose a unified interpretation for the high mass-to-light ratios in galaxy clusters and the rotation curves of galaxies.

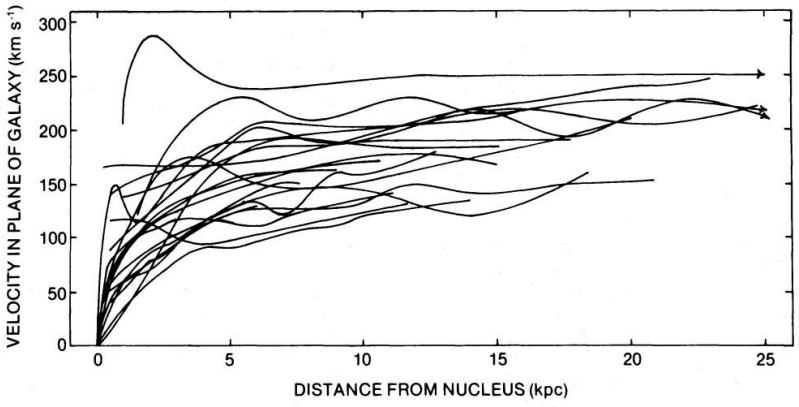

Figure 1.1: The radial velocity of several galaxies as a function of the distance to the nucleus, from the original paper of Vera Rubin

1.1.3 Cosmic Microwave Background

The study conducted by the Planck satellite on the anisotropies in the Cosmic Microwave Background (CMB), particularly its angular power spectrum, determined the total matter density fraction, $\Omega_m = 0.1326 \pm 0.0063$, and the baryonic density fraction, $\Omega_b = 0.02273 \pm 0.0006$. The parameter Ω is defined as ρ/ρ_c, where ρ is the current matter density of the Universe, and ρ_c is the critical density required for the Universe to be spatially flat.
In this context, "matter" refers to all material with the same equation of state as dust, characterized by $p = 0$. This includes both baryonic matter and Dark Matter, which are assumed to have the same equation of state. For each type of matter (with its own equation of state), there is an associated density fraction Ω_i (see Appendix A.1).
We can distinguish between Ω_m and Ω_b because baryonic matter interacts with the photon bath (i.e., the electromagnetic field), whereas Dark Matter does not. For baryonic matter, if a region of higher density forms due to statistical fluctuations, gravitational effects that would enhance this density are counteracted by electromagnetic interactions. Dark Matter, on the other hand, does not experience these interactions, leading to different effects on the angular power spectrum of the CMB.
Additionally, the ratio between baryonic matter and Dark Matter is consistent with what we expect to explain the velocities of galaxies within clusters and the velocities of stars within galaxies. Finally, the CMB provides insights into the era of its formation, even predating the formation of stars and galaxies. This evidence strongly suggests the presence of a type of matter that influenced the Universe's history from its early stages, does not interact with the photon bath, and has a density approximately five times greater than that of baryons.

1.1.4 Cosmological Scales

As pointed out in the CMB paragraph, the presence of Dark Matter favored the growth of inhomogeneities in our universe. We understand very well how cosmological structures formed: the tiny perturbations we observed in the CMB grew under the influence of gravity and generated the large-scale structure that we observe today. Nevertheless, it can be shown that this growth is quite weak in a radiation-dominated universe, and it is still too slow when matter dominates. Furthermore, since before the CMB era, baryonic matter and the photon bath were tightly coupled, this model is not completely accurate. In fact, baryonic perturbations can grow only after the time of recombination when the Universe becomes neutral and photons decouple. It has been proved that, with only baryonic matter today, we would have a much smoother and more homogeneous universe compared to our current universe. To have the high inhomogeneities and cosmological structures we observe today, we need some species that decoupled from the baryon-photon plasma much earlier than recombination, creating gravitational potential wells. At recombination, baryons finally decouple from photons and fall into these potential wells formed earlier, which allows the perturbations to grow faster. Fur-

thermore, from the study of the matter power spectrum—a quantity that measures matter density fluctuations at different scales—we can learn about the necessity of Dark Matter: The predictions obtained by accounting for Dark Matter are very successful. Without Dark Matter, the theoretical predictions would be very different, leading to significant disagreement with observations.

1.1.5 Other Evidence

- Gravitational lensing consists of the bending of light rays due to nearby massive objects and can be used to infer the presence of mass between us and what we observe. Both galaxies and clusters of galaxies act as gravitational lenses. We refer to strong lensing when the lens produces multiple images of the same object. In contrast, weak lensing occurs when the lens merely distorts the image of the source. By studying gravitational lensing caused by galaxies, we can determine the gravitational mass of the object and infer the structure of the halos around galaxies. Gravitational lensing confirms the existence of Dark Matter halos around galaxies and reveals the presence of enormous quantities of Dark Matter in galaxy clusters.
- There are example, like in the Bullet Cluster and MACS J0018.5, where the baryonic matter and the gravitational potential appear clearly spatially separated. In the Bullet Cluster, baryonic matter was detected through X-rays, while the gravitational potential well was mapped using weak gravitational lensing.
- While Big Bang Nucleosynthesis (BBN) does not provide direct evidence for Dark Matter, it predicts the abundances of light elements and thereby provides a measurement of baryon density. The results from BBN are consistent with observations from the CMB and are smaller than the total matter density, suggesting the presence of Dark Matter.

1.2 What do we know about Dark Matter?

Dark Matter has attractive gravitational interactions and is either stable or has a lifetime much longer than the age of the Universe. This is almost tautological: we postulate the existence of Dark Matter, assuming that the theory of gravity is correct, to explain the motion of baryonic matter inside galaxy clusters and galaxies.
One might then wonder, as anticipated in the preface, whether we could abandon the postulate of Dark Matter and instead consider that the law of gravity might be incorrect. This is the goal of theories known as MOND (MOdified Newtonian Dynamics).
We will now explore this possibility in more detail. The first such theory was proposed in 1982 by Mordehai Milgrom. He suggested replacing Newton's second law $F = ma$ with $F = \mu(a)ma$, where $\mu(a)$ deviates from 1 only for very small accelerations a, specifically $a \ll a_0 \simeq 1.2 \times 10^{-10}$ m/s^2. In this regime, $\mu = a/a_0$, and from the modified second law of Newton:

$$F = \frac{GMm}{r^2} = ma\mu = \frac{ma^2}{a_0} \tag{1.7}$$

We obtain:

$$a = \frac{\sqrt{GMa_0}}{r} \tag{1.8}$$

From the centripetal acceleration $a = v^2/r$, we derive $v = (GMa_0)^{1/4}$.
This correction to the theory of gravity would explain why rotation velocity curves remain flat at large distances from the center of a galaxy, instead of decreasing, without the need to assume the existence of Dark Matter. However, this theory, as originally postulated, has some problems. Firstly, it is unclear from Milgrom's articles whether his theory modifies the law of gravity or corrects Newton's second law. Additionally, this theory does not conserve energy, linear momentum and angular momentum. Finally, MOND is a non-relativistic theory and thus cannot be applied where General Relativity is required.
Therefore, to consider MOND a viable alternative to Dark Matter, a more refined version of the theory

was needed. For this reason, Jacob Bekenstein developed the TeVeS theory (short for Tensor-Vector-Scalar gravity) in 2004. This theory is embedded in a relativistic framework and modifies only the law of gravity.
TeVeS is compatible with the observed rotation curves of hundreds of spiral galaxies and also explains the empirical Tully-Fisher law, which relates the intrinsic luminosities and rotational velocities of spiral galaxies, $L \propto V^{\alpha}$ where $\alpha \simeq 4$.
However, TeVeS fails to explain observations at the scale of galaxy clusters. Although MOND reduces the need for additional mass in clusters, significant quantities of Dark Matter are still required.
Furthermore, TeVeS does not account for the observation of two merging galaxy clusters, collectively named the Bullet Cluster, which we mentioned in 1.1.

1.2.1 Mass

The mass of the main component of Dark Matter has been constrained within a broad range of about 80 orders of magnitude. A firm upper bound is established: $m_{DM} \leq 2 \times 10^{-9}$ $M_{\odot} = 2 \times 10^{48}$ GeV. This constraint arises from the unsuccessful search for MACHOs, very massive and compact objects that were considered viable candidates up until the late 1980s.
The proposed strategy involved monitoring large numbers of stars in nearby galaxies to detect variations in their brightness. If MACHOs were responsible for the halo, we would have expected to observe a certain number of microlensing events, but these were never detected. By the mid-1990s, it became clear that compact objects did not seem to account for the missing mass, at least not in the Milky Way's halo. During this period, various surveys (including those by the Kepler satellite, and the ground-based MACHOS and EROS collaborations) and theoretical considerations ruled out mass ranges greater than 2×10^{48} GeV.
The lower limit on the Dark Matter particle mass is less well defined and depends on the nature of Dark Matter and its statistical properties. To explain the existence of small Dark Matter-dominated structures, such as dwarf galaxies with typical sizes of $R \simeq 1$ kpc, Dark Matter must be able to localize within these galaxies. For bosons, the de Broglie wavelength of the Dark Matter particle must be smaller than the size of these dwarf galaxies. Using a typical velocity, and the Heisenberg uncertainty principle, this leads to the constraint $m_{DM} > 10^{-22}$ eV. For fermions, the constraint is more stringent. The Pauli exclusion principle limits the number of particles that can fit into different structures, such as dwarf galaxies. Knowing the Dark Matter mass for these objects allows us to determine the lower limit for fermions to be between 0.2 and 0.7 keV, assuming these particles reached thermal equilibrium in the early universe.

1.2.2 Charge Neutrality

We know that Dark Matter does not interact with light. In fact, it does not absorb, emit, or reflect light at any frequency, which indicates that Dark Matter has a very small electromagnetic coupling. There are hypotheses that the "dark sector"—the collection of particles that make up Dark Matter (which could include more than one type of particle)—might contain "millicharged Dark Matter" particles that couple with the Standard Model via a "dark photon."
Observational upper limits on the cross section for elastic Dark Matter-photon interactions are currently set at $\sigma_{DM-\gamma} \leq 4 \times 10^{-33}$ cm^2. Additionally, we have bounds on the charge of Dark Matter: $q < 10^{-6}$ for $m_{DM} = 10$ GeV and $q < 10^{-4}$ for $m_{DM} = 10$ TeV.
One important consequence of Dark Matter's weak interaction with light is that it cannot cool by radiating photons during galaxy formation.
This also explains the presence of extended dark halos around galaxies; if Dark Matter could cool like baryonic matter, it would collapse at the center of disk galaxies.
While most of Dark Matter is dissipationless, some part of it could be dissipative. This would imply the formation of a second "dark disk" on galactic scales, a concept behind Partially Interacting Dark Matter (PIDM). The formation of such a dark disk would provide strong evidence in favor of this model. PIDM could emit dark photons or other dark particles.

1.2.3 Self Interaction

For simplicity, Dark Matter has traditionally been assumed to be collisionless. However, studies of systems like the Bullet Cluster indicate that the upper bound for the self-interaction cross-section is quite significant, $\sigma_{self}/m \leq 2$ barns/GeV.
There are indeed models that propose Self-Interacting Dark Matter (SIDM) to address and resolve the cuspy-core problem. This problem arises from the discrepancy between simulations of N-body systems and the observed density profiles of Dark Matter halos around galaxies. Specifically, observations reveal uniform regions of Dark Matter around dwarf galaxies, whereas simulations had predicted a steeper density distribution. Another possible explanation for this issue is a model involving a mix of cold and warm Dark Matter.

1.2.4 Coldness

We call Cold, Warm and Hot Dark matter according to the typical velocity of Dark Matter. As already said, to explain the structure of our Universe, we need Dark Matter. In fact, baryonic matter can only form after recombination, which is when atoms become stable. Before this, photon pressure prevents the formation of stable atoms.
Once stable atoms are formed, they must fall into an existing gravitational well; otherwise, there would not be enough time to form the structures of the Universe that we observe today. Numerical simulations show that if Dark Matter had relativistic velocities, the structures at the galaxy scale would be washed out, meaning we wouldn't observe galaxies. For Warm Dark Matter, the smallest-scale structures are dwarf galaxies. Both Cold and Warm Dark Matter (respectively CDM and WDM) can account for all large-scale structure observations. The primary difference between them appears at the dwarf-galaxy scale, where observations and interpretations are still inconclusive.
It is important to note that the density profiles of Dark Matter inside galactic halos do not match those predicted by CDM-only simulations. One possible solution is the presence of WDM alongside CDM, or incorporating baryonic matter more fully in simulations.
We also note that neutrinos, which had been considered a promising candidate for Dark Matter until the 1980s, are excluded as Dark Matter candidates because they are relativistic, hence, Hot Dark Matter (HDM) is not considered capable of forming the structures in our Universe. We will revisit this point in the next chapter
Finally the relic abundance of Dark Matter and its primordial velocity distribution are tightly constrained by cosmological assumptions made about the thermal history of the Universe. If we identify a Dark Matter particle from this thermal history, its properties could serve as a cosmological probe to gain information about that epoch.

1.2.5 Stability

We conclude this chapter by discussing the stability of Dark Matter. We know that Dark Matter was already present during the formation of the CMB and remains around galaxies and inside galaxy clusters. This implies that the most stable particle in the dark sector has a lifetime comparable to the age of the universe. Nevertheless, the strongest bounds on the lifetime of Dark Matter are stronger: $\tau_{DM} > 10^{18}$ s for non-visible products (i.e., those not interacting with the electromagnetic field), and $\tau_{DM} > 10^{25-29}$ s when the products are visible.

Chapter 2

Instantaneous Freeze-Out

We can divide Dark Matter candidates into "thermal" and "non-thermal" relics. Thermal relics are produced during the early stages of the universe while in equilibrium with a thermal bath. They reach equilibrium with this bath and then, at a certain point, "decouple" or "freeze-out" when their interactions can no longer keep up with the expansion of the universe. Chemical equilibrium is disrupted when the reactions altering the number of particles occur slower than the universe's expansion rate, after which the number of particles per comoving volume remains constant.
When this happens, we say they have chemically decoupled. However, at a certain point, they also kinetically decouple. After kinetic decoupling, the exchange of momentum with the radiation bath ceases to be effective.
As we will see, the transition from thermal equilibrium is the process that sets the relic density we observe today. All other options fall into non-thermal models.
To maintain thermal equilibrium with the radiation bath, we need to assume the existence of an interaction between the dark sector and the particles of the Standard Model. The simplest interaction we can consider is:

$$\chi\overline{\chi} \rightarrow \psi\overline{\psi} \tag{2.1}$$

where χ represents the Dark Matter particle and ψ represents a Standard Model particle. This equation shows that two Dark Matter particles annihilate to produce two Standard Model particles.
We define the rate of annihilation as $\Gamma_{ann} = n_\chi \langle \sigma v_{M\o l} \rangle$, where the angle brackets indicate the average over all possible states of the colliding particles. Here, $v_{M\o l}$ is the Møller velocity (see A.2) between χ and $\overline{\chi}$, and σ is the cross section of the interaction.
As mentioned earlier, we expect that at some point a particle species decouples from the thermal bath, and subsequently, the number of particles of that species freezes out. If the temperature of the species is $T_{FO} > m_\chi$ at freeze-out, we refer to this as relativistic freeze-out; otherwise, it is called non-relativistic freeze-out. Using the instantaneous freeze-out model, we estimate that Dark Matter particles decoupled when:

$$\Gamma_{ann}(T_{FO}) = n_\chi \langle \sigma v_{M\o l} \rangle = H(T_{FO}) \tag{2.2}$$

Here, we compare the rate of annihilation of Dark Matter particles with the rate of expansion of the universe, represented by the Hubble constant H. Both rates depend on the temperature of the thermal bath, and for a certain temperature T_{FO}, we expect them to be equal. When $H(T_{FO}) > \Gamma_{ann}(T_{FO})$, the universe's expansion is so rapid that it prevents two Dark Matter particles from interacting and annihilating.
Before proceeding, we derive some results useful for studying this model for both Hot and Cold Dark Matter. From Friedmann's equation (A.4), we can show that when the scale factor a is small (i.e., at the early stages of the universe), we have a radiation-dominated universe. As discussed in the section on Friedmann's equations, $\rho_r = 3H^2/8\pi G$. Additionally, from statistical mechanics considerations, we have $\rho_r = \frac{\pi^2}{30} g_*(T) T^4$, where the subscript r indicates a radiation-dominated universe, and g_* counts the total number of effectively massless degrees of freedom in the Standard Model (see A.3). From

this, we can derive the value of H:

$$H(T) = \frac{\pi}{3}\sqrt{\frac{8\pi G}{10}}\sqrt{g_*(T)}T^2 \tag{2.3}$$

Note that $1/\sqrt{8\pi G}$ is the Planck Mass, M_{Pl}, in natural units.

2.1 Relativistic Freeze-Out

In this section, we focus on relativistic freeze-out, specifically the case where Dark Matter decouples from the thermal bath when it is relativistic: $T_{FO} > m_\chi$. We proceed by using the instantaneous freeze-out model, and thus we apply the expression given in 2.2 and the expression for the Hubble constant in a radiation-dominated universe. In this context, the expression for n_χ is given by:

$$n_\chi = g_{eff}\frac{\zeta(3)}{\pi^2}T^3 \tag{2.4}$$

Where $g_{eff} = g_\chi$ for bosons and $g_{eff} = \frac{3}{4}g_\chi$ for fermions, and $\zeta(z)$ is the Riemann zeta function. Using this expression, we get:

$$g_{eff}\frac{\zeta(3)}{\pi^2}T_{FO}^3\langle\sigma v_{M\o l}\rangle = \frac{\pi}{3}\sqrt{\frac{g_*(T_{FO})}{10}}\frac{T_{FO}^2}{M_{Pl}} \tag{2.5}$$

So we can easily compute T_{FO}:

$$T_{FO} = \frac{\pi^3}{3\zeta(3)\sqrt{10}}\frac{g_*(T_{FO})}{g_{eff}}\frac{1}{\langle\sigma v_{M\o l}\rangle M_{Pl}} \tag{2.6}$$

Obviously, this is correct as long as $T_{FO} \gg m_\chi$. With this result, one can compute $n_\chi(T_{FO})$, and to calculate $\Omega_\chi h^2$, we introduce a quantity that we will use again in 3.
After freeze-out, the number of Dark Matter particles remains constant (in the first approximation), and thus the number density of Dark Matter evolves as $n_\chi \propto a^{-3}$. This also implies that the comoving number density remains constant (defined as the number of particles per unit of comoving volume). We can compute its value at freeze-out since it does not change afterward. For an adiabatic expansion, the total entropy of the universe remains constant, so $S = sa^3$ is conserved, which means that $s \propto a^{-3}$. Defining the variable $Y_\chi = n_\chi/s$, it is proportional to the number of particles per comoving volume na^3. Then the relic density is:

$$\Omega_\chi h^2 = \frac{\rho_\chi}{\rho_{crit}/h^2} = \frac{m_\chi Y_\chi(T_{FO})s_0}{\rho_{cirt}/h^2} \tag{2.7}$$

Where the numerator in the density associated with χ, $\rho_{crit} \simeq 1.05\times10^{-5}h^2$ GeV cm^{-3}, is the critical density required for the universe to be flat, and $s_0 \simeq 2.9\times10^3$ cm^{-3} is the entropy per comoving volume today. To compute Y_χ, we use 2.4 and $s(T_{FO}) = \frac{2\pi^2}{45}g_{*s}(T_{FO})T_{FO}^3$, where g_{*s} is the effective number of degrees of freedom for entropy. (see A.3).
We now suppose $\sigma^2 \simeq G_F^2T^2$. This expression is valid for weak interactions, where $G_F \simeq 10^{-5}/\text{GeV}^2$ is the Fermi constant and represents the cross section of neutrinos. From this expression, one obtains that $T_{FO} = O(\text{MeV})$. Finally, by substituting the numerical values, we get:

$$\Omega_\chi h^2 \simeq 0.076\left(\frac{g_{eff}}{g_{*s}(T_{FO})}\right)\left(\frac{m_\chi}{eV}\right) \tag{2.8}$$

If we impose $\Omega_\chi h^2 \simeq 0.12$, we find the Cowisk-McClelland relation:

$$m_\chi \simeq 168.55eV\frac{1}{g_{eff}}\left(\frac{g_{*s}(T_{FO})}{106.75}\right) \tag{2.9}$$

Thus, for HDark Matter, we would have $m_\chi = 10 - 100$ eV. Nevertheless, as seen in Chapter 1, Hot Dark Matter cannot explain the formation of structures at galactic scales.

2.2 Non-relativistic Freeze-Out

We now explore the case of Cold Dark Matter, specifically the scenario where Dark Matter decouples from the thermal bath when it is non-relativistic: $T_{FO} < m_\chi$. For a species of non-relativistic particles ($m \gg T$) that remains in thermal equilibrium, we expect their number density to be:

$$n_\chi = g_\chi \left(\frac{m_\chi T}{2\pi}\right)^{3/2} e^{-m_\chi/T} \tag{2.10}$$

Where g_χ represents the internal degrees of freedom of the Dark Matter particles. Note that because of the exponential factor, if Dark Matter always remained in equilibrium with the thermal bath, its number density would be approximately zero as T approaches some Kelvins. We can now through 2.10 rewrite 2.2, using the change of variable $x_{FO} = m_\chi/T_{FO}$:

$$e^{-x_{FO}} \frac{g_\chi m_\chi^3}{(2\pi)^{3/2}} x_{FO}^{-3/2} \langle \sigma v_{M\o l} \rangle = \frac{\pi}{3M_{Pl}} \sqrt{\frac{g_*(x_{FO})}{10}} \frac{m_\chi^2}{x_{FO}^2} \tag{2.11}$$

We find the freeze-out temperature solving numerically this equation. Taking the logarithm on both sides:

$$x_{FO} = \frac{1}{2} \ln x_{FO} + \ln \left(\frac{g_\chi}{\sqrt{g_*(T_{FO})}}\right) + \ln \left(m_\chi \langle \sigma v_{M\o l} \rangle M_{Pl}\right) + \ln \left(\frac{3\sqrt{5}}{2\pi^{5/2}}\right) \tag{2.12}$$

We note that the freeze-out temperature T_{FO} depends weakly (logarithmically) on m_χ and $\langle \sigma v_{M\o l} \rangle$. Moreover, in this case, for small velocities, we can Taylor expand: $\sigma v = a + bv^2 + O(v^4)$. Taking the average over a thermal distribution, we set $\langle \sigma v_{M\o l} \rangle$ as constant (corresponding to an s-wave). As reference values, we take $m_\chi = 100$ GeV and $\langle \sigma v_{M\o l} \rangle = 1$ pb $\approx 2.6 \times 10^{-9} \text{GeV}^{-2}$ (but the same result holds for similar values) and get:

$$x_{FO} \simeq \frac{1}{2} \ln(x_{FO}) + \ln \left(\frac{g_\chi}{\sqrt{g_*(T_{FO})}}\right) + 25 \tag{2.13}$$

This means that, up to minor corrections, $x_{FO} \simeq 25$. Obviously, to compute x_{FO} with better accuracy, we need to make some assumptions about the number of degrees of freedom of Dark Matter, g_χ, and we need to know the dependence of g_* on T (see A.3). If we let T vary over a wide range of temperatures, from 10^{-2} GeV to 10^6 GeV, g_* ranges between 10 and 100, so $x_{FO} \simeq 25$ is a solid estimate over this range. It is important to note as a consistency check that $x_{FO} \simeq 25$ implies $T_{FO} \ll m_\chi$, which is the hypothesis from which we started. As done for relativistic freeze-out, one can compute $Y_\chi(T_{FO})$ and then, using 2.7, compute $\Omega_\chi h^2$:

$$\Omega_\chi h^2 \simeq 2.09 \times 10^8 \frac{g_*^{1/2}(T_{FO})}{g_{*s}(T_{FO})} \frac{x_{FO}}{M_{Pl} \langle \sigma v_{M\o l} \rangle} \text{ GeV}^{-1} \tag{2.14}$$

This expression is valid for any value of m_χ and $\langle \sigma v_{M\o l} \rangle$ if the freeze-out happens in the non-relativistic regime. We plug in $x_{FO} = 25$ and impose $g(T_{FO}) = g_s(T_{FO})$, which is true except at very low temperatures. After working through the numbers, we obtain:

$$\Omega_\chi h^2 \simeq 0.12 \left(\frac{106.75}{g(T_{FO})}\right)^{1/2} \left(\frac{0.7, \text{pb}}{\langle \sigma v_{M\o l} \rangle}\right) \tag{2.15}$$

Where the numbers within the brackets are typical values for $g(T_{FO})$ at $T_{FO} \simeq 200$ GeV and for $\langle \sigma v_{M\o l} \rangle$ in processes mediated by weak interactions. The value $\Omega_{DM} = 0.12$ is highlighted. This expression leads us to conclude that, for these values, we would obtain the correct relic density of Dark Matter. This is remarkable because it means that WIMPs predict the correct value of Ω_{DM}, making them excellent Dark Matter candidates for masses in the GeV-to-TeV range. This is sometimes referred to as "the WIMP miracle." However, we must not be deceived; having two parameters means you can always adjust one to achieve the correct relic density.

Chapter 3

Boltzmann Equation

Departures from thermal equilibrium lead to varying relic densities for different types of particles, including Dark Matter candidates. Once a species decouples from the thermal bath, its comoving density stops evolving and remains roughly constant. Instantaneous freeze-out assumes perfect thermal equilibrium before decoupling, with the comoving density remaining constant afterward.
However, this is only an approximation. The transition between these two regimes is smoother, so to analyze it properly, we need a new tool: the Boltzmann equation.
To properly track the decoupling process, we must follow the microscopic evolution of the particle's phase space distribution $f(p^\mu, x^\mu)$, where p^μ represents the four-momentum of the particle and is defined as the derivative of the space-time coordinates with respect to an affine parameter. Furthermore, p^μ must satisfy the on-shell relation $p^\mu p_\mu = p^\mu g_{\mu\nu} p^\nu = m_\chi^2$, where $g_{\mu\nu}$ is the Robertson-Walker metric (see appendix A.1) but could be any metric. We now present the Boltzmann equation:

$$\hat{\mathbf{L}}[f] = \hat{\mathbf{C}}[f] \tag{3.1}$$

Here, $\hat{\mathbf{L}}$ is the Liouville operator, and $\hat{\mathbf{C}}$ is the collision operator. The left-hand side of the equation represents the evolution of the phase space distribution due to the geometry of space-time, while the right-hand side accounts for the effects of decays and production processes.

3.1 The Liouville Operator

The Liouville operator $\hat{\mathbf{L}}$ is the total derivative of the phase space density with respect to an affine parameter:

$$\hat{\mathbf{L}}[f] = \frac{d}{d\lambda} f(x^\mu, p^\mu) = \left[\frac{dx^\mu}{d\lambda} \frac{\partial}{\partial x^\mu} + \frac{dp^\mu}{d\lambda} \frac{\partial}{\partial p^\mu} \right] f \tag{3.2}$$

Without any interactions, particles move along space-time geodesics, and we can substitute the derivative of the four-momentum $dp^\mu/d\lambda$ using the geodesics equation. We also recognize $dx^\mu/d\lambda$ as the four-momentum. We can rewrite $\hat{\mathbf{L}}$ as:

$$\hat{\mathbf{L}}[f] = \left[p^\mu \frac{\partial}{\partial x^\mu} - \Gamma^\mu_{\alpha\beta} p^\alpha p^\beta \frac{\partial}{\partial p^\mu} \right] f \tag{3.3}$$

Where $\Gamma^\mu_{\alpha\beta}$ is the affine connection. As stated before we are using the Robertson-Walker metric and so we expect the phase space density to be spatially homogeneous and isotropic. The homogeneity in space imposes that the derivatives of f with respect to spatial coordinates are vanishing and so the first term in the right-hand side is equal to:

$$p^\mu \frac{\partial}{\partial x^\mu} = E \frac{\partial}{\partial t} \tag{3.4}$$

While using the non-vanishing affine connection of the Robertson-Walker metric, we can rewrite the second term. Putting all together, we get:

$$\hat{\mathbf{L}}[f] = E\frac{\partial f}{\partial t} - H(E^2 - m_\chi^2)\frac{\partial f}{\partial E} \tag{3.5}$$

Using the definition of n_χ:

$$n_\chi = g_\chi \int f(E,t)\frac{d^3p}{(2\pi)^3} \tag{3.6}$$

To compute the Boltzmann equation it is cost-effective to integrate this expression over d^3p and multiply by g_χ/E.

$$g_\chi \int \left(\frac{\partial f}{\partial t} - H\frac{|p|^2}{E}\frac{\partial f}{\partial E}\right)\frac{d^3p}{(2\pi)^3} = \frac{dn_\chi}{dt} - g_\chi H \int \frac{|p|^2}{E}\frac{\partial f}{\partial E}\frac{d^3p}{(2\pi)^3} \tag{3.7}$$

We now compute this integral:

$$g_\chi \int \frac{|p|^2}{E}\frac{\partial f}{\partial E}\frac{d^3p}{(2\pi)^3} = g_\chi \int \frac{|p|^2}{E}\frac{\partial p}{\partial E}\frac{\partial f}{\partial p}\frac{d^3p}{(2\pi)^3} = g_\chi \int |p|\frac{\partial f}{\partial p}\frac{d^3p}{(2\pi)^3} \tag{3.8}$$

We can now evaluate this integral using spherical coordinates:

$$g_\chi \frac{4\pi}{(2\pi)^3}\int_0^{+\infty} |p|^3\frac{\partial f}{\partial p} = g_\chi \frac{4\pi}{(2\pi)^3}\left(p^3 f|_0^{+\infty} - 3\int_0^{+\infty}|p|^2 f\right) \tag{3.9}$$

The first term vanishes because we assume f vanishes faster than $|p|^3$ and the last term is just three times n_χ in spherical coordinates (from 3.6). Combining these, we obtain the left-hand side of the Boltzmann equation as:

$$\frac{dn_\chi}{dt} + 3Hn_\chi \tag{3.10}$$

This equation tells us that the number density of χ, in the absence of interactions, is only affected by the dilution effect of the expansion of the universe. In fact, as we will show, if $\hat{\mathbf{C}}$=0, then $n_\chi a^3$ is constant, as expected.

3.2 The Collision Operator

We can now focus on the collision operator $\hat{\mathbf{C}}$ for generic a process:

$$\chi + a + b + \ldots \longleftrightarrow i + j + \ldots \tag{3.11}$$

As already done for the Liouville operator it is helpful to integrate $\hat{\mathbf{C}}$ over the phase space, we will call this integral $\mathcal{C}$:

$$\begin{aligned}\mathcal{C} = \frac{g_\chi}{(2\pi)^3}\int \hat{\mathbf{C}}[f]\frac{d^3p_\chi}{E_\chi} = -\int & d\Pi_\chi d\Pi_a d\Pi_b \cdots d\Pi_i d\Pi_j \cdots \\ & \times (2\pi)^4\delta^4(p_\chi + p_a + p_b + \ldots - p_i - p_j - \ldots) \\ & \times [|\mathcal{M}_\rightarrow|^2 f_a f_b f_\chi \cdots (1 \pm f_i)(1 \pm f_j)\cdots \\ & \quad - |\mathcal{M}_\leftarrow|^2 f_i f_j \cdots (1 \pm f_\chi)(1 \pm f_a)(1 \pm f_b)\cdots]\end{aligned} \tag{3.12}$$

Here, $|\mathcal{M}|$ is the matrix element averaged over initial and final spins and includes any symmetry factors for identical particles. The right arrow corresponds to the direct process in 3.11, while the left arrow denotes the inverse reaction.
We now focus on the reaction given in 2.1. In the early universe, where $f \ll 1$, we can approximate $1 \pm f \simeq 1$. Assuming CP (or T) invariance, we also have $|\mathcal{M}\rightarrow| = |\mathcal{M}\leftarrow|$. Within these hypotheses the generic expression 3.12 takes the following form:

$$\mathcal{C} = -\int (2\pi)^4 \delta^4(p_\chi + p_{\bar{\chi}} - p_\psi - p_{\bar{\psi}}), d\Pi_\chi, d\Pi_{\bar{\chi}}, d\Pi_\psi, d\Pi_{\bar{\psi}} |\mathcal{M}|^2 (f_\chi f_{\bar{\chi}} - f_\psi f_{\bar{\psi}}) \tag{3.13}$$

We assume that the process in 2.1 occurs with perfect symmetry between χ and $\overline{\chi}$, as well as between ψ and $\overline{\psi}$. Specifically, we assume that ψ represents all the species into which χ annihilates and that it is in thermal equilibrium. This is because these particles have additional interactions with the thermal bath that are stronger than their interactions with χ. Given that ψ is in thermal equilibrium and assuming zero chemical potential (while the Boltzmann equation remains covariant, with this assumption, we are now choosing a specific frame of reference), its distribution is given by $f_\psi = \exp[-E_\psi/T]$. The delta function then provides us with the relation $E_\chi + E_{\overline{\chi}} = E_\psi + E_{\overline{\psi}}$. From these expressions, we can write:

$$f_\psi f_{\overline{\psi}} = exp[-(E_{\overline{\psi}} + E_\psi)/T] = exp[-(E_\chi + E_{\overline{\chi}})/T] = f_\chi^{eq} f_{\overline{\chi}}^{eq} \tag{3.14}$$

We will use:

$$f_i(E,t) = \frac{n_i(t)}{n_i^{eq}} f_i^{eq}(E,t) \tag{3.15}$$

With f_i^{eq} the distribution for species i in thermal equilibrium. We also define the thermally averaged cross section:

$$\langle \sigma v_{M\o l} \rangle = (n_\psi^{eq})^{-2} \int (2\pi)^4 \delta^4(p_\chi + p_b - p_c - p_d) \;\; d\Pi_b d\Pi_c d\Pi_d d\Pi_\chi \; |\mathcal{M}|^2 e^{-(E_\psi + E_{\bar{\psi}})/T} \tag{3.16}$$

Where n^{eq} is the number density at thermal equilibrium. With this definition we can rewrite 3.13 as:

$$\mathcal{C} = -\langle \sigma v_{M\o l} \rangle [n_\chi^2 - (n_\chi^{eq})^2] \tag{3.17}$$

We can finally write the Boltzmann equation:

$$\frac{dn_\chi}{dt} + 3Hn_\chi = -\langle \sigma v_{M\o l} \rangle [n_\chi^2 - (n_\chi^{eq})^2] \tag{3.18}$$

In the Boltzmann equation (3.18) the thermal average $\langle \sigma v_{M\o l} \rangle$ has usually been done by expanding the cross section at low relative velocity. However, there are cases, such as near a resonance or a threshold, where the cross section is poorly approximated by this expansion or where it may even become divergent.

3.3 Thermal Average

For the definition, we have that $\langle \sigma v_{M\o l} \rangle$, for an equilibrium Maxwell-Boltzmann distribution at temperature T, i.e., $f(E) \propto \exp(-E/T)$, is:

$$\langle \sigma v_{M\o l} \rangle = \frac{\int \sigma v_{M\o l} e^{-E_1/T} e^{-E_2/T} d^3p_1 d^3p_2}{\int e^{-E_1/T} e^{-E_2/T} d^3p_1 d^3p_2} \tag{3.19}$$

Particle 1 and 2 in our case are just the colliding particles χ and $\bar{\chi}$. We can rewrite the momentum-space volume element:

$$d^3p_1 d^3p_2 = 4\pi p_1 E_1 dE_1 \; 4\pi p_2 E_2 dE_2 \; \frac{1}{2} dcos\theta \tag{3.20}$$

Where θ is the angle between the three-momenta and we used the shell equation. Changing variables:

$$E_+ = E_1 + E_2, \qquad E_- = E_1 - E_2, \qquad s = 2m^2 + 2E_1E_2 - 2p_1p_2cos\theta \tag{3.21}$$

We obtain $d^3p_1 d^3p_2 = 2\pi^2 E_1 E_2 dE_+ dE_- ds$. The integration region $\{E_1 > m,\ E_2 > m,\ |cos\theta| < 1\}$ transforms in:

$$|E_-| \leq \sqrt{1 - \frac{4m^2}{s}} \sqrt{E_+^2 - s}, \qquad E_+ \geq \sqrt{s}, \qquad s \geq 4m^2 \tag{3.22}$$

Once this is done we can rewrite the numerator of 3.19:

$$\begin{aligned}\int \sigma v_{M\o l} e^{-E_1/T} e^{-E_2/T} d^3p_1 d^3p_2 &= 2\pi^2 \int dE_+ \int dE_- \int ds \sigma v_{M\o l} E_1 E_2 e^{-E_+/T} = \\ &= 2\pi^2 \int ds \sigma(s-4m^2) \int dE_+ e^{-E_+/T} \sqrt{E_+^2 - s} = \\ &= 2\pi^2 T \int ds \sigma(s-4m^2) \sqrt{s} K_1(\sqrt{s}/T).\end{aligned} \tag{3.23}$$

Where we used A.16 and K_i is the modified Bessel function of the second kind of order i. The denominator is: [1]:

$$\int e^{-E_1/T} e^{-E_2/T} d^3p_1 d^3p_2 = [4\pi m^2 T K_2(m/T)]^2 \tag{3.24}$$

Putting all together we rewrite 3.19:

$$\langle \sigma v_{M\o l} \rangle = \frac{\int_{4m^2}^{+\infty} ds \sigma(s-4m^2)\sqrt{s} K_1(\sqrt{s}/T)}{8Tm^4 K_2^2(m/T)} \tag{3.25}$$

This result is valid for Maxwell-Boltzmann statistics, but for $T < m/3$ (from confronting the rest mass energy with the thermal energy) it can be safely applied to all statistics. To perform this integral, it is convenient to switch to a frame of reference different from the comoving frame. We will now demonstrate this statements, where the first equality is used to perform the integral:

$$\langle \sigma v_{M\o l} \rangle = \langle \sigma v_{lab} \rangle^{lab} \neq \langle \sigma v_{cm} \rangle^{cm} \tag{3.26}$$

The first quantity is the thermal average of $\sigma v_{M\o l}$ in the comoving reference frame, while the other quantities will be specified later. We now use $v_{M\o l} = v_{rel}(1 - \mathbf{v}1 \cdot \mathbf{v}2)$ (from A.2), where v_{rel} is the relative velocity between particle 1 and particle 2, and $\mathbf{v}1$ and $\mathbf{v}2$ are the velocities of particle 1 and particle 2 in the comoving reference frame. Since v_{rel} is an invariant, the Møller velocity transforms according to the following law:

$$v_{M\o l} = v'_{M\o l} \frac{(1 - \mathbf{v}1 \cdot \mathbf{v}2)}{(1 - \mathbf{v}1' \cdot \mathbf{v}2')} \tag{3.27}$$

where the prime indicates quantities in the new reference frame.
We now define the lab frame as the rest frame of one of the incoming particles. In this case, from A.2, $v_{M\o l}^{lab} = v_{lab}$, where v_{lab} is just the velocity of the incoming particle in the lab frame, while the velocity of the other particle vanishes. Thus, from 3.27, we get $v_{M\o l} = v_{lab}(1 - \mathbf{v}1 \cdot \mathbf{v}2)$.
Let's now define the Møller velocity in the center-of-mass frame (c.m. frame). In this case, $v_{M\o l}^{cm} = v_{cm}$, and by multiplying and dividing by $p_1^\mu p_{2\mu}$, one gets:

$$v_{M\o l} = v'_{M\o l} \frac{(1 - \mathbf{v}_1 \cdot \mathbf{v}_2)}{(1 - \mathbf{v}'_1 \cdot \mathbf{v}'_2)} = v_{cm} \frac{1}{2} \frac{2E_1^{cm} E_2^{cm}}{E_1 E_2} \tag{3.28}$$

And:

$$v_{M\o l} = v_{cm} \frac{1}{2} \left(\frac{E_1^{cm} E_2^{cm} + p^2 + m^2}{E_1 E_2} \right) = v_{cm} \frac{1}{2} \left(\frac{p_1^\mu p_{2\mu} + m^2}{E_1 E_2} \right) = v_{cm} \frac{1}{2} \left(1 - \mathbf{v}_1 \cdot \mathbf{v}_2 + \frac{m^2}{E_1 E_2} \right) \tag{3.29}$$

Where we used the modulus of the tri-momentum p in the c.m. frame. We can now proceed with the definition of the thermal average in the primed frame:

$$\langle \sigma v'_{M\o l} \rangle = \frac{\int \sigma v'_{M\o l} dn'_1 dn'_2}{\int dn'_1 dn'_2} \tag{3.30}$$

[1] To compute the numerator one has just to use the definition of the Bessel function with an easy change of variables, while for the denominator to use the propriety $\frac{\partial K_1}{\partial z} = \frac{K_1}{z} + K_2$.

For definition of Møller velocity the numerator is invariant (see section A.2) while the denominator changes because of the contraction of volumes, as seen before. This means that are valid the equalities:

$$\langle \sigma v_{M\o l} \rangle = \langle \sigma v'_{M\o l} \rangle' \left\langle \frac{V_1 V_2}{V_1' V_2'} \right\rangle = \langle \sigma v'_{M\o l} \rangle' \left\langle \frac{E_1' E_2'}{E_1 E_2} \right\rangle = \langle \sigma v'_{M\o l} \rangle \left\langle \frac{v_{M\o l}}{v'_{M\o l}} \right\rangle \tag{3.31}$$

The thermal averages for the lab and c.m. frames are respectively:

$$\left\langle \frac{v_{M\o l}}{v_{lab}} \right\rangle = \langle 1 - \mathbf{v}_1 \cdot \mathbf{v}_2 \rangle = 1, \quad \left\langle \frac{v_{M\o l}}{v_{cm}} \right\rangle = \frac{1}{2} \left[1 + \left\langle \frac{m^2}{E_1 E_2} \right\rangle \right] = \frac{1}{2} \left[1 + \frac{K_1^2(x)}{K_2^2(x)} \right] \tag{3.32}$$

Where for the lab frame the average is taken for all possible angles $\mathbf{v}_1$ and $\mathbf{v}_2$ and for the c.m. frame For sake of brevity we present only the result without the derivation. We rewrite the result as:

$$\langle \sigma v_{M\o l} \rangle = \langle \sigma v_{lab} \rangle^{lab} = \frac{1}{2} \left[1 + \frac{K_1^2(x)}{K_2^2(x)} \right] \langle \sigma v_{M\o l} \rangle \tag{3.33}$$

Using the numerical values of the modified Bessel functions of the second kind, we find that for $x \to 0$, which corresponds to relativistic freeze-out, $\langle v_{M\o l}/v_{cm} \rangle \to 1/2$. In contrast, for $x \to \infty$, representing non-relativistic freeze-out, the asymptotic expansion gives $\langle v_{M\o l}/v_{cm} \rangle \to 1$. Specifically, for the case we are interested in, where $x \simeq 20 - 25$, we find that $\langle v_{M\o l}/v_{cm} \rangle \simeq 0.932 - 0.945$.
Since $\langle \sigma v_{M\o l} \rangle = \langle \sigma v_{lab} \rangle^{lab}$, it is convenient to perform the integral in the lab frame. To do this, we use the kinetic energy per unit mass in the lab frame, given by $\epsilon = (s - 4m^2)/4m^2$.
Using the shell relation and the fact that $v = p/E$, one can also show that $v_{lab} = \frac{2\sqrt{\epsilon(1+\epsilon)}}{1+2\epsilon}$. Thus, we can rewrite 3.25 as:

$$\langle \sigma v_{M\o l} \rangle = \int_0^\infty d\epsilon \, \mathcal{K}(x, \epsilon) \, \sigma v_{lab}, \qquad \mathcal{K}(x, \epsilon) = \frac{2x}{K_2^2(x)} \sqrt{\epsilon}(1 + 2\epsilon) K_1(2x\sqrt{1+\epsilon}) \tag{3.34}$$

Once the value of σv_{lab} is known, the integral can be computed numerically, which avoids the potential complications associated with expanding σv_{lab} in powers of ϵ.
In some cases, it is useful to compute the thermal average of $\sigma v_{M\o l}$ in the non-relativistic limit. Here, the relativistic Maxwell-Boltzmann distribution ($\propto e^{-E/T}$) in 3.19 is replaced by the non-relativistic Maxwell-Boltzmann distribution ($\propto e^{-p^2/2mT}$).
In this non-relativistic case, the denominator of 3.19 is straightforward to compute and yields $(2\pi m T)^3$. For the numerator, we use the integration variables $\mathbf{p}_{rel} = \mathbf{p}_1 - \mathbf{p}_2$ and $\mathbf{p}_{tot} = \mathbf{p}_1 + \mathbf{p}_2$. Since $\sigma v_{M\o l}$ depends only on $\mathbf{p}_{rel}$, we can perform the integral over $\mathbf{p}_{tot}$. After some calculations, we obtain:

$$\langle \sigma v_{M\o l} \rangle_{n.r.} = \frac{2x^{3/2}}{\pi^{1/2}} \int_0^\infty \sigma v_{lab} \epsilon^{1/2} e^{-x\epsilon}, d\epsilon \tag{3.35}$$

Where $p_{rel}^2 = 4m^2\epsilon$. Outside of resonances or thresholds, we can safely Taylor expand σv_{lab} in powers of ϵ and use this expansion to compute the integral 3.34 or 3.35. Specifically, in the first case, one should use the expansion of the Bessel functions for large arguments. We do not delve into all the computational details, but it is worth noting that they coincide only up to the first order. There is particularly better agreement if σv_{lab} is a slow function of ϵ. Typically, for cold relics (in our case $x \simeq 20 - 25$), if we consider a non-relativistic distribution, we are committing an error of about $\simeq 1 - 5\%$.

3.4 Semi-Analytical Solutions

It is advantageous to express 3.18 in terms of dimensionless quantities. To achieve this, we first employ the comoving number density Y_χ, as defined previously in 2, to account for the effects of cosmic expansion:

$$\frac{dY_\chi}{dt} = \frac{d}{dt} \left[\frac{n_\chi a^3}{s a^3} \right] = \frac{1}{s a^3} \left[a^3 \frac{dn_\chi}{dt} + 3a^2 n_\chi \frac{da}{dt} \right] = \frac{1}{s} \left[\frac{dn_\chi}{dt} + 3H n_\chi \right] \tag{3.36}$$

Where we used the conservation of entropy per comoving volume. We can then rewrite the Boltzmann equation 3.18 in the following way:

$$\frac{dY_\chi}{dt} = -s\langle\sigma v_{M\o l}\rangle(Y_\chi^2 - (Y_\chi^{eq})^2) \tag{3.37}$$

Where we used $n_\chi = Y_\chi s$. Then we define the dimensionless variable $x = m_\chi/T$. It is convenient rewrite dY_χ/dt as it follows:

$$\frac{dY_\chi}{dt} = \frac{dY_\chi}{dx}\frac{dx}{dt} \tag{3.38}$$

We now want to properly express dx/dt. From the conservation of the entropy in a comoving volume we have $S = \frac{2\pi^2}{45} g_{*s} T^3 a^3 = const.$ then:

$$0 = \frac{d}{dt}\left[g_{*s}\left(\frac{a}{x}\right)^3\right] = \frac{a^3}{x^3}\frac{dg_{*s}}{dx}\frac{dx}{dt} + \frac{3a^2}{x^3} g_{*s}\dot{a} - \frac{3a^3}{x^4}\frac{dx}{dt} g_{*s} \tag{3.39}$$

Simplifying common factors, calling $dg_{*s}/dx = g_{*s}^{'}$ and $H = \dot{a}/a$ we get:

$$\frac{dx}{dt} = \frac{Hx}{1 - \frac{x}{3}\frac{g_{*s}^{'}}{g_{*s}}} \tag{3.40}$$

We then can rewrite the Boltzmann in its final form:

$$\frac{dY_\chi}{dx} = -\langle\sigma v_{M\o l}\rangle\frac{s}{Hx}\left(1 - \frac{x}{3}\frac{g_{*s}^{'}}{g_{*s}}\right)(Y_\chi^2 - (Y_\chi^{eq})^2) \tag{3.41}$$

To give a semi-analytical solution for the Boltzmann equation we take $g_{*s} = const.$ With this assumption made we arrive at this differential equation:

$$\frac{dY_\chi}{dx} = -\langle\sigma v_{M\o l}\rangle\frac{s}{Hx}(Y_\chi^2 - (Y_\chi^{eq})^2) \tag{3.42}$$

This form of the Boltzmann equation is an ordinary differential equation quadratic in the independent variable and there are not closed analytical solutions. Before giving a semi-analytical solution we first need to express the x dependence of s and H. As pointed out earlier in 2 $H(x) = H(x=1)x^{-2}$ and $s(x) = s(x=1)x^{-3}$. We can then rewrite:

$$\frac{dY_\chi}{dx} = -\frac{\lambda}{x^2}\left[Y_\chi^2 - (Y_\chi^{eq})^2\right], \qquad \lambda := \frac{s(x=1)\langle\sigma v_{M\o l}\rangle}{H(x=1)} \tag{3.43}$$

We define $\Delta_\chi = Y_\chi - Y_\chi^{eq}$:

$$\frac{d\Delta_\chi}{dx} = -\frac{dY_\chi^{eq}}{dx} - \frac{\lambda}{x^2}\ \Delta_\chi(2Y_\chi^{eq} + \Delta_\chi) \tag{3.44}$$

Before freeze-out, Δ_χ is nearly zero. Therefore we can impose $d\Delta_\chi/dx = 0$. Solving for Δ_χ, we get:

$$\Delta_\chi = \frac{x^2}{\lambda[\Delta_\chi + 2Y_\chi^{eq}]}\frac{dY_\chi^{eq}}{dx}, \qquad x < x_{FO} \tag{3.45}$$

While long after the freeze-out we have that that Y_χ^{eq} becomes negligible, and thus $Y_\chi \simeq \Delta_\chi$. Consequently, we obtain:

$$\frac{d\Delta_\chi}{dx} = -\frac{\lambda}{x^2}\Delta_\chi^2, \qquad x > x_{FO} \tag{3.46}$$

This differential equation is easily solved, allowing us to determine Y_χ^0, where the suffix denotes the present value:

$$Y_\chi^0 = \left(\int\frac{\lambda}{x^2}dx\right)^{-1} = \sqrt{\frac{45}{\pi}}\frac{g_*^{1/2}}{g_{*s}}\frac{1}{mM_{Pl}}\frac{1}{J(x_{FO})} \quad ; \quad J(x_{FO}) = \int_{x_{FO}}^{\infty} dx\frac{\langle\sigma v_{M\o l}\rangle}{x^2} \tag{3.47}$$

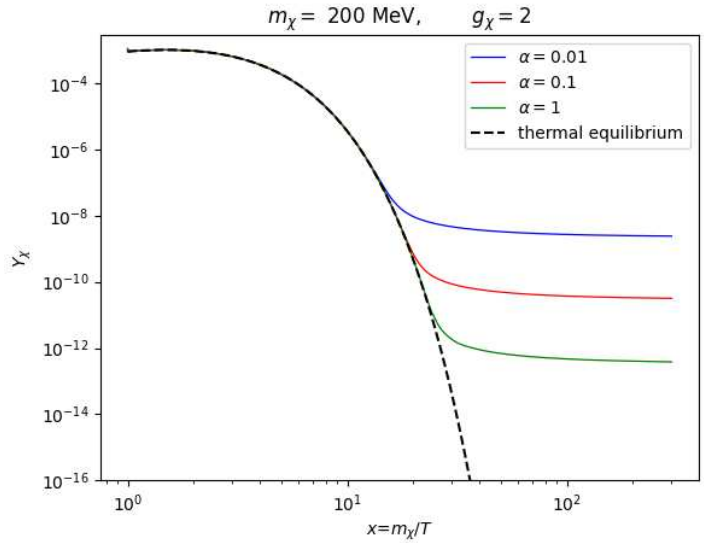

Figure 3.1: Numerical solutions of the Boltzmann equation for three different values of α, the dashed line represents the density per comoving value for a specie in thermal equilibrium

This can also be rewritten in the following way:

$$\frac{1}{Y_\chi^0} = \frac{1}{Y_\chi^{FO}} + \left(\frac{45}{\pi}G\right)^{1/2} \int_{T_0}^{T_{FO}} \frac{g_{*s}}{\sqrt{g_*}} \langle \sigma v_{M\o l} \rangle dT \tag{3.48}$$

Where we used $dT = -dx\ m/x^2$, and in the first case we neglected $1/Y_\chi^{FO}$. From this we can compute easily the relic density using 2.7:

$$\Omega_\chi h^2 = \frac{1.07 \times 10^9 GeV^{-1}}{g_*^{1/2} M_{Pl} J(x_{FO})} \tag{3.49}$$

We note that by providing an expression for $\langle \sigma v_{M\o l} \rangle$ using a Taylor expansion, as discussed in 3.3, we can evaluate $J(x_{FO})$ and compute the relic density. This approach yields, at first order, the same result for both the relativistic and non-relativistic regimes:

$$\Omega_\chi h^2 = \frac{1.07 \times 10^9 GeV^{-1} x_{FO}}{g_*^{1/2} M_{Pl} (a^{(0)} + 3a^{(1)}/x_{FO})} \tag{3.50}$$

Where $a^{(n)}$ indicates the nth derivative of $\sigma v_{M\o l}$ with respect to ϵ evaluated at $\epsilon = 0$.
Using the expression for the Hubble constant in a radiation-dominated universe and the expression for the entropy, we can rewrite λ. Additionally, we need to specify $\langle \sigma v_{M\o l} \rangle$ as well.

$$\lambda = \frac{2\pi\sqrt{10}}{15} m_\chi M_{Pl} \frac{g_{*s}}{\sqrt{g_*}} \langle \sigma v_{M\o l} \rangle \tag{3.51}$$

We remark that we are neglecting the dependence of g_{*s} and g_* on x. We choose the annihilation cross section to be: $\langle \sigma v_{M\o l} \rangle = \frac{\alpha_\chi^2}{32\pi m_\chi^2}$. This cross section is selected to represent an s-wave process, which is typical for weak interactions (on the order of pb). We set $m_\chi = 200$ GeV and in addition, we compare three different values of the coupling α_χ. In figure 3.1 we observe several important points: First, the line representing thermal equilibrium approaches zero, indicating that, in the absence of decoupling, the relic density of Dark Matter would be zero. Second, there is a specific point at which Y_χ decouples from the thermal bath. The decoupling occurs at different values of x for different values of α_χ; however, in all cases, $x_{FO} \simeq$ 20-30. As anticipated, for larger values of the cross section, decoupling occurs at a later time, resulting in a lower relic density ($\Omega_\chi \propto 1/\sigma$).

Chapter 4

Annihilation Near Poles

In this section, we consider the case where annihilation takes place near a pole or a resonance in the cross section. This can happen, for example, when there is an s-channel exchange of a mediator particle with mass approximately twice the Dark Matter mass. Let m be the mass of the colliding particles, m_R the mass of the resonance, and Γ_R its width. We now consider a resonant cross section of the relativistic Breit-Wigner form:

$$\sigma_{res} = \frac{4\pi\omega}{p^2} B_i B_f \frac{m_R^2 \Gamma_R^2}{(s - m_R^2)^2 + m_R^2 \Gamma_R^2} \tag{4.1}$$

Here, $\omega = (2J+1)/(2S+1)^2$ is a statistical factor, S is the spin of the colliding particles, J is the spin of the resonance, $p = \frac{1}{2}(s - 4m^2)^{1/2}$ is the center-of-mass momentum, and B_i and B_f are the branching fractions of the resonance into the initial and final channel, respectively. We rewrite the cross section in a more convenient way as follows, using ϵ defined in 3.3, $\gamma_R = m_R \Gamma_R / 4m^2$ and $\epsilon_R = (m_R^2 - 4m^2)/4m^2$.

$$\sigma_{res} = \frac{4\pi\omega}{m^2 \epsilon} B_i B_f \frac{\gamma_R^2}{(\epsilon - \epsilon_R)^2 + \gamma_R^2} \tag{4.2}$$

Using $v_{lab} = 2\sqrt{\epsilon(1+\epsilon)}/(1+2\epsilon)$ and $B_f = 1 - B_i$, we can write:

$$\sigma_{res} v_{lab} = \frac{8\pi\omega}{m^2} \frac{\gamma_R^2}{(\epsilon - \epsilon_R)^2 + \gamma_R^2} b_R(\epsilon) \tag{4.3}$$

Where the factor $b_R(\epsilon)$ is given by:

$$b_r(\epsilon) = \frac{B_i(1 - B_i)(1+\epsilon)^{1/2}}{\epsilon^{1/2}(1+2\epsilon)} \tag{4.4}$$

And we assume that $b_R(\epsilon)$ is a very slow function of ϵ near the resonance, (i.e., far from $\epsilon = 0$) and it can be expanded in powers of ϵ:

$$b_R(\epsilon) = \sum_{l=0}^{\infty} \frac{b_R^{(l)}}{l!} \epsilon^l \tag{4.5}$$

We now firstly examine the case where we have a very narrow resonance, $\gamma_R << 1$. Recalling the relation

$$\lim_{\gamma \to 0} \quad \frac{\gamma}{x^2 + \gamma^2} = \pi \delta(x) \tag{4.6}$$

We write:

$$\sigma_{res} v_{lab} = \frac{8\pi^2 \omega}{m^2} \gamma_R \delta(\epsilon - \epsilon_R) b_R(\epsilon_R) \tag{4.7}$$

Using this expression we can compute using 3.34 the relativistic thermal average:

$$\langle \sigma_{res} v_{m\o l} \rangle = \frac{16\pi^2 \omega}{m^2} \frac{x}{K_2^2(x)} \gamma_R B_i (1 - B_i) \sqrt{1 + \epsilon_R} K_1(2x\sqrt{1+\epsilon_R}) \theta(\epsilon_R) \tag{4.8}$$

While the non-relativistic formula (3.35) gives:

$$\langle \sigma_{res} v_{m\not{o}l} \rangle_{n.r.} = \frac{16\pi\omega}{m^2} x^{3/2} \pi^{1/2} \gamma_R \epsilon_R^{1/2} e^{-x\epsilon_R} b_R(\epsilon_R) \theta(\epsilon_R) \tag{4.9}$$

Here, $\theta(\epsilon_R)$ represents the Heaviside function. In fact the integral for the thermal average is performed for $\epsilon > 0$, which means that if $\epsilon_R < 0$—i.e., if the particle mass exceeds half the resonance mass m_R—a narrow resonance does not contribute to the thermally averaged cross section. This is because, in the center-of-mass frame, the resonance must be formed at rest, and if $m > m_R$, energy conservation would require the resonance to have momentum, leading to a contradiction. Conversely, when $m < m_R$, there are collisions, driven by the thermal distribution, with sufficient energy to form the resonance. While this holds for a very narrow resonance, a broader one may still contribute to the thermal average of the cross section even when $m > m_R$. Generally, particles with a mass greater than $(m_R + \Gamma_R)/2$ have too much rest energy to produce a resonance.
For arbitrary values of Γ_R, the relativistic average must be computed numerically, but a closed-form expression can be obtained for the non-relativistic case. We will first present some analytical results for the non-relativistic thermal average, followed by numerical computations for both relativistic and non-relativistic averages. We can write 4.3 as it follows:

$$\langle \sigma_{res} v_{lab} \rangle = \frac{8\pi\omega}{m^2} \gamma_R \ \mathrm{Re} \ \frac{i}{\epsilon_R + i\gamma_R - \epsilon} b_R(\epsilon) \tag{4.10}$$

Using the non-relativistic thermal average (3.35) we can write:

$$\langle \sigma_{res} v_{m\not{o}l} \rangle_{n.r.} = \frac{16\pi^{1/2}\omega}{m^2} x^{3/2} \gamma_R \int_0^\infty \mathrm{Re} \, \frac{\epsilon^{1/2} e^{-x\epsilon}}{z_R - \epsilon} b_R(\epsilon) d\epsilon \tag{4.11}$$

Where $z_R = \epsilon_R + i\gamma_R$. We can expand $b_R(\epsilon)$, swap the summation with the integral sign, and rewrite it as:

$$\langle \sigma_{res} v_{m\not{o}l} \rangle_{n.r.} = \frac{16\pi\omega}{m^2} x^{3/2} \gamma_R \pi^{1/2} \sum_{l=0}^{\infty} \frac{b_R^{(l)}}{l!} F_l(z_R; x) \tag{4.12}$$

Where we define:

$$F_l(z_R; x) = \mathrm{Re} \, \frac{i}{\pi} \int_0^\infty \frac{\epsilon^{l+1/2} e^{-x\epsilon}}{z_R - \epsilon} d\epsilon \tag{4.13}$$

By passing the derivative inside the integral sign and differentiating the exponential, it is easy to show the following relation:

$$F_l(z_R; x) = -\frac{\partial}{\partial x} F_{l-1}(z_R; x) \tag{4.14}$$

And thus:

$$F_l(z_R; x) = (-1)^l \frac{\partial^l}{\partial x^l} F_0(z_R; x) \tag{4.15}$$

And through some computations it can be also showed that:

$$F_0(z_R; x) = \mathrm{Re} \left(z_R^{1/2} e^{-z_R x} \, \mathrm{erfc}(-i x^{1/2} z_R^{1/2}) \right) \tag{4.16}$$

With these formulae we can approximate $\langle \sigma_{res} v_{m\not{o}l} \rangle_{n.r.}$ up to any order.

We now present some numerical results for the thermal average of $\sigma v_{M\not{o}l}$. It is important to note that the thermal average depends on both $2m/m_R$ and x. Although we could have shown a single 3D surface plot, for clarity and readability, we instead present two 2D sections of the same plot. In 4.1, we present the thermal average of $\sigma v_{M\not{o}l}$ as a function of $2m/m_R$ for two values of x, computed using both relativistic and non-relativistic averages. The non-relativistic average shows a steeper function, and, as expected, for larger values of x, the relativistic and non-relativistic thermal averages show better agreement. We also note that the relativistic thermal average presents broadened peaks and shifted towards bigger masses due to the thermal distributions.

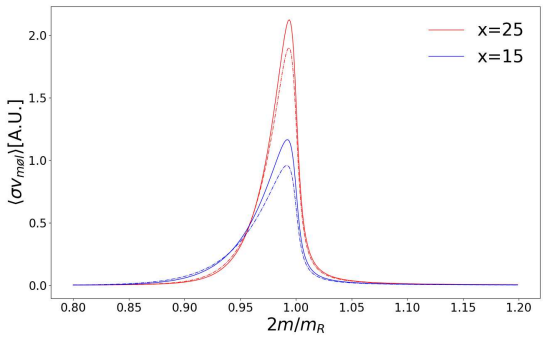

Figure 4.1: The dashed lines represent the relativistic thermal average of $\sigma v_{M\phi l}$, while the solid lines correspond to the non-relativistic thermal averages. Red lines are for $x = 25$, and blue lines are for $x = 15$. In all cases, $\gamma_R = 0.01$.

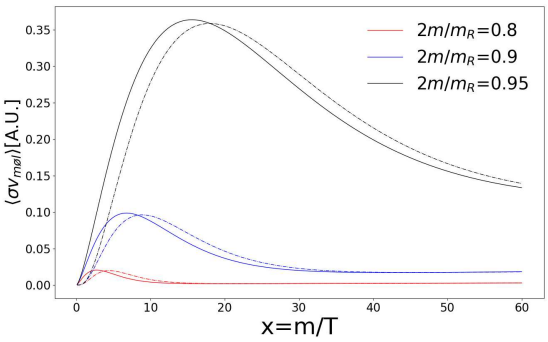

Figure 4.2: The dashed lines represent the relativistic thermal average, while the solid lines correspond to the non-relativistic thermal averages. Black lines refer to $2m/m_R = 0.95$, blue lines to $2m/m_R = 0.90$, and red lines to $2m/m_R = 0.80$. In all cases, $\gamma_R = 0.01$.

In 4.2, we present the thermal average as a function of x for three different values of $2m/m_R$. These functions are used to calculate J_χ and, consequently, the relic density. Specifically, one needs to integrate the functions shown in 4.2, divided by x^2, from x_{FO} to infinity. Note that the units used on the y-axis of both 4.1 and 4.2 are $B_i B_f 8\pi\gamma_R^2\omega/m^2$.
In 4.3, we present the computation of Ω_χ using both relativistic and non-relativistic thermal averages for two different values of γ_R. The relic density was computed by integrating from $x_{FO} = 25$ to $x = 500$. While ideally, the integration should extend from x_{FO} to infinity, we limited it to $x = 500$ due to numerical constraints. This approximation introduces an error of about 5%. Extending the integration domain would not significantly change the trend of the graph, also due to the logarithmic scale used. We opted to limit the integration range to highlight both relativistic and non-relativistic results.
Note that the logarithmic scale on the y-axis may obscure differences between the two types of thermal averages too, but the graphs indicate good agreement between the relativistic and non-relativistic computations. The unit used on the y-axis is 1.07×10^9 GeV$^{-1} \times 25, B_i B_f 8\pi\gamma_R^2\omega/(m^2 M_{Pl} g_*^{1/2})$. We finally observe a striking suppression of the relic density near the resonance, with a reduction factor of approximately 10^3 for $\gamma_R = 0.03$ and 10^4 for $\gamma_R = 0.01$. This result clearly demonstrates how the presence of a resonance in the cross-section can significantly impact the relic density of Dark Matter. This finding will be further discussed in the conclusions.

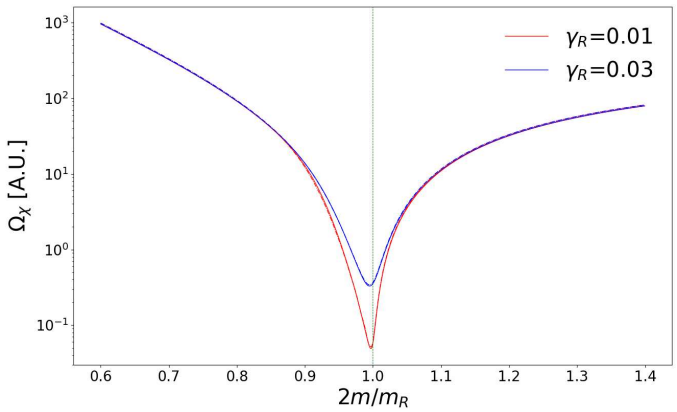

Figure 4.3: Ω_χ as a function of $2m/m_R$ for two different values of γ_R. The red lines correspond to $\gamma_R = 0.01$, while the blue lines correspond to $\gamma_R = 0.03$. Dashed lines represent the relativistic average, and solid lines represent the non-relativistic thermal average.

Conclusions

In this work we first described the observational evidences that led to the formulation of the existence of Dark Matter. We then focused on the WIMPs model and what we can say about them. Among all the models, we analyzed the model of thermal Dark Matter. As previously discussed, thermal Dark Matter presupposes the existence of an interaction with Standard Model particles that allows it to maintain thermal equilibrium with the primordial plasma. It has then been studied that, due to the expansion of the universe, such interactions are insufficient to maintain thermal equilibrium, leading to the decoupling of Dark Matter from the thermal bath and resulting in the freeze-out. This process was initially studied using an instantaneous freeze-out model and later through the Boltzmann equation.
Subsequently, it was studied how to perform the thermal averaging of the generic cross-section that describes the interaction between Dark Matter and the Standard Model, which is a necessary quantity for studying the freeze-out. We finally focused on the specific case where Dark Matter particles annihilate close to a resonance, and we provided an explicit expression for the cross section. Applying what we learned, we calculated the thermal average of the cross section, which allowed us to determine how it influences the relic density. What we found is that near a resonance, the relic density is significantly suppressed. This is particularly important: indeed, thermal Dark Matter, being a testable model, has been the subject of various experiments aimed at detecting its interaction with ordinary matter, which is presumed to exist. The lack of detection has imposed stringent limits on the cross section, specifically upper limits. It has been observed that this implies lower limits on the relic density ($\Omega_\chi \propto 1/\sigma$), and if these limits were greater than Ω_{DM} =0.12, it would lead to the falsification of the model.
If, on the other hand, we assume the presence of resonances in the cross section, we can achieve small relic densities even with small couplings values, thanks to the suppression mentioned earlier. This therefore allows us to still consider thermal Dark Matter as a reasonable paradigm for explaining Dark Matter.

Appendix A

Useful Results

A.1 Friedmann's Equations

The cosmological principle asserts that the Universe is homogeneous and isotropic. This "principle" is actually an empirical fact, and happens to be true only at the large scales of the Universe: extremely large galaxy surveys such as the 2dF Galaxy Redshift Survey and the Sloan Digital Sky Survey revealed that there are not any huge structure on scales greater than hundreds of Mpc, to give an idea of this enormous scale, the radius of our galaxy is about $\simeq 12.5$ kpc, the nearest galaxy of similar size to our own, the Andromeda Galaxy, is at a distance of about 800 kpc. The typical distance between galaxies of the size of the Milky Way is about $\simeq 1$ Mpc. We add that the biggest structures in the universe are galaxy clusters or superclusters with a typical size that ranges from 1-15 Mpc to $\simeq 100$ Mpc.
The cosmological principle justifies the assumption that our Universe, at least at these large scales, can be described by the Robertson–Walker metric, the most general metric for a spacetime that is spatially homogeneous and isotropic, but evolving in time:

$$ds^2 = -c^2dt^2 + a^2(t)\left(\frac{dr^2}{1-kr^2} + r^2d\Omega^2\right) \tag{A.1}$$

Where $a(t)$ is a function of time and is called the scale factor of the Universe. k is a constant that gives us information about the curvature of the Universe: if $k > 0$, we live in a spherical geometry world; if $k = 0$, we live in a flat world; and if $k < 0$, in a hyperbolic geometry. We remark that r, θ, and ϕ are often called comoving coordinates: regardless of what $a(t)$ is doing, their values remain the same (for non-moving particles). Given this metric, we can write the Einstein field equations:

$$G_{\mu\nu} = \frac{8\pi G}{c^4}T_{\mu\nu} \tag{A.2}$$

Where $G_{\mu\nu}$ is the Einstein tensor and $T_{\mu\nu}$ is the stress-energy tensor. We underline that the Einstein tensor is dependent only on the metric, so given the metric one can always compute it. For the sake of brevity, we do not show it explicitly.
What Einstein's equation is telling us is how the presence of matter curves spacetime, and so we have to describe the matter under consideration. We choose to model matter in the Universe by a perfect fluid at rest. In this case:

$$T^\mu_\nu = diag(-\rho c^2, p, p, p) \tag{A.3}$$

We have raised an index to get a convenient form of the stress-energy tensor. Plugging in T^ν_μ and computing the Einstein tensor, one gets only 2 independent equations:

$$\left(\frac{\dot{a}}{a}\right)^2 + \frac{kc^2}{a^2} = \frac{8\pi G}{3}\rho \tag{A.4}$$

And:

$$2\left(\frac{\ddot{a}}{a}\right) + \left(\frac{\dot{a}}{a}\right)^2 + \frac{kc^2}{a^2} = -8\pi G\frac{p}{c^2} \tag{A.5}$$

Equation A.4 is the first Friedmann equation, subtracting A.4 to A.5 we get the second Friedmann equation:

$$\frac{\ddot{a}}{a} = -\frac{4\pi G}{3}(\rho + 3p) \tag{A.6}$$

We notice that we have three functions of time: $a(t)$, $\rho(t)$, and $p(t)$. If we want to solve for these functions and get an explicit dependence on time, we will need one more equation; namely, we need an equation of state, which gives the relation between ρ and p. In fact, taking the derivative with respect to time in A.4 and using A.6, we get:

$$\dot{\rho} + 3\left(\frac{\dot{a}}{a}\right)(\rho + p) = 0 \tag{A.7}$$

If we use an equation of state in the form $\rho = wp$ where w is a constant that depends on the type of the matter we arrive at:

$$\frac{\dot{\rho}}{\rho} = -3(1+w)\frac{\dot{a}}{a} \tag{A.8}$$

So we obtain that $\rho \propto a^{-3(1+w)}$. For different types of matter, we can choose different values of w. For baryonic matter and Dark Matter, we set $w = 0$, which implies $p = 0$, allowing us to think of them as dust in the vacuum, without any pressure. Consequently, we have $\rho \propto a^{-3}$. This also means that:

$$\frac{d}{dt}(a^3\rho) = 0 \tag{A.9}$$

This equation states the intuitive fact that if the content of matter in the universe doesn't change, then its density is diluted as the volume of the universe increases.
From statistical mechanics considerations for radiation, we have $w = \frac{1}{3}$, so $\rho \propto a^{-4}$. This can also be explained intuitively: the density of photons scales as a^{-3} and their energy as a^{-1}, since $E_\gamma = \frac{hc}{\lambda}$ and $\lambda \propto a$. We conclude with the definition of the Hubble parameter H:

$$H = \frac{\dot{a}}{a} \tag{A.10}$$

The value of the Hubble parameter at the present epoch is the Hubble constant, H_0, and it is roughly 70 ± 10 km/sec/Mpc.

A.2 Møller Velocity

In this section, we focus on the meaning of $v_{M\o l}$. In the non-relativistic regime, $v_{M\o l}$ is simply the relative velocity between the colliding beams of particles. However, when relativistic corrections are taken into account, this is no longer true.
We start with the rate of collisions occurring in volume dV over time dt for two beams of particles with number densities n_1 and n_2. In the reference frame in which particle 2 is at rest, the rate of collisions is given by $d\nu = \sigma v_{rel} n_1 n_2 dV dt$, where $d\nu$ is, by its nature, an invariant quantity. In a generic reference frame, we get $d\nu = A n_1 n_2 dV dt$.
Here, A is a quantity to be determined, but we know that $A = \sigma v_{rel}$ in the rest frame of particle 2. In addition being both $d\nu$ and $dVdt$ invariant quantities, we get that An_1n_2 is invariant too. We will always use the cross section σ in the rest frame of a particle, so σ is an invariant quantity. We note that if:

$$A = \sigma v_{rel}\frac{p_{1\mu}p_2^\mu}{E_1E_2} \tag{A.11}$$

We get the correct expression for A in the rest frame of particle 2 and An_1n_2 is invariant. We now give an expression to get v_{rel}. In an arbitrary reference frame particle 1 and 2 have velocities $\mathbf{v}_1$ and $\mathbf{v}_2$ respectively. From $p_{1\mu}p_2^\mu$ computed in the rest frame of particle 2 we obtain v_{rel}:

$$p_{1\mu}p_2^\mu = \frac{m_1m_2}{\sqrt{1-v_{rel}^2}} \qquad \Rightarrow \qquad v_{rel} = \sqrt{1 - \frac{m_1^2m_2^2}{(p_{1\mu}p_2^\mu)^2}} \tag{A.12}$$

In any reference frame $p_{1\mu}p_2^\mu = E_1E_2 - \mathbf{p}_1 \cdot \mathbf{p}_2$. Using $v = E/p$ and $E = m/\sqrt{1-v^2}$ we get:

$$p_{1\mu}p_2^\mu = m_1m_2\frac{1-\mathbf{v}_1\cdot\mathbf{v}_2}{\sqrt{(1-v_1^2)(1-v_2^2)}} = E_1E_2(1-\mathbf{v}_1\cdot\mathbf{v}_2) \tag{A.13}$$

Substituting in A.12, after simple computations, we get:

$$v_{rel} = \frac{\sqrt{(\mathbf{v}_1-\mathbf{v}_2)^2 - (\mathbf{v}_1\times\mathbf{v}_2)^2}}{1-\mathbf{v}_1\cdot\mathbf{v}_2} \tag{A.14}$$

We can now substitute A.11 and A.14 to compute the collision rate. After some algebraic manipulations, we obtain the collision rate in an arbitrary frame of reference:

$$d\nu = \sigma\sqrt{(\mathbf{v}_1-\mathbf{v}_2)^2 - (\mathbf{v}_1\times\mathbf{v}_2)^2}n_1n_2dVdt \tag{A.15}$$

It is very common to define the Møller velocity $v_{M\o l} \equiv \sqrt{(\mathbf{v}_1-\mathbf{v}_2)^2 - (\mathbf{v}_1\times\mathbf{v}_2)^2}$.
In this way, the expression for the rate of collision per unit volume and time is similar to the non-relativistic expression: $d\nu = \sigma v_{M\o l}n_1n_2dVdt$. From this, it is easy to see that, to compute Γ, one must use the Møller velocity.
We finally derive a result that will be useful in the next section, we want to show that:

$$v_{M\o l}E_1E_2 = \sqrt{\frac{1}{4}s(s-4m^2)} \tag{A.16}$$

Using A.12 and A.13:

$$v_{M\o l}E_1E_2 = v_{rel}E_1E_2(1-\mathbf{v}_1\cdot\mathbf{v}_2) = \sqrt{1-\frac{m_1^2m_2^2}{(p_{1\mu}p_2^\mu)^2}}(p_{1\mu}p_2^\mu) \tag{A.17}$$

From this is only matter of algebraic computations to show equation A.16

A.3 Degrees of Freedom

In this section we provide a more precise definition of g_* and g_{*s} and examine how the dependence of degrees of freedom on temperature influences the Boltzmann equation. We assume that each species of particles i in the early universe is in kinetic equilibrium, with a well-defined temperature T_i. We can express its energy and entropy as follows:

$$\begin{aligned}\rho_i(T_i) &= \int f(T_i,E_i)E_i d^3p_i \\ s_i(T_i) &= \int \frac{3m_i^2+4p_i^2}{3E_iT_i}f(T_i,E_i)d^3p_i\end{aligned} \tag{A.18}$$

Here, we use $s = (\rho+P)/T$, where $P = p^2/E$ is the pressure of the gas. Recall that the distribution function $f(E_i,T_i)$ is given by:

$$f(E_i,T_i) = \frac{g_i}{(2\pi)^3}\frac{1}{\exp(E_i/T_i)+\eta_i} \tag{A.19}$$

With $\eta_i = 1$ for Fermi-Dirac statistics, $\eta_i = -1$ for Bose-Einstein statistics, and $\eta_i = 0$ for Maxwell-Boltzmann statistics, and g_i denoting the number of internal degrees of freedom for the particle species, we now define the *effective* degrees of freedom for energy and entropy:

$$g_{*,i}(T) = \frac{30}{\pi^2T^4}\rho_i(T) = \frac{15g_i}{\pi^4}x_i^4\int_1^\infty \frac{y^2(y^2-1)^{1/2}}{\exp(x_iy)+\eta_i}dy \tag{A.20}$$

$$g_{*s,i}(T) = \frac{45}{2\pi^2T^3}s_i(T) = \frac{45g_i}{4\pi^4}x_i^4\int_1^\infty \frac{y(y^2-1)^{1/2}}{\exp(x_iy)+\eta_i}\frac{4y^2-1}{3y}dy \tag{A.21}$$

Where the integrals in A.18 are performed in spherical coordinates ($d^3p = 4\pi E\sqrt{E^2 - m^2}\, dE$) with the coordinate change $y = E/m$.
The contributions of each species to the total number of effective degrees of freedom for entropy and energy are weighted by $g^{(i)} = g_{*,i}\left(\frac{T_i}{T}\right)^4$ and $g_s^{(i)} = g_{*s,i}\left(\frac{T_i}{T}\right)^3$, respectively.
Each species contributes to the total energy density ρ and entropy density s with its own ρ_i and s_i, at its own temperature T_i. To express ρ and s in terms of the temperature of the thermal bath T rather than T_i, we need to define these effective numbers of degrees of freedom.
The total effective degrees of freedom for energy and entropy are denoted g_* and g_{*s}, respectively, and are the sum of these weighted contributions. Note that in general, $g^{(i)} \neq g_{*,i}$ (or $g_s^{(i)} \neq g_{*s,i}$).
In principle, by knowing the temperature of each species of particles and their respective number of effective degrees of freedom, one can always compute g_* and g_{*s}. This can also be done by exploiting the fact that up to decoupling, the temperature of the thermal bath T and the temperature of each species T_i are the same.
We will not go into the details here but will illustrate how the number of degrees of freedom is affected by temperature: In particular, studying the thermal history of the universe and observing A.1, we

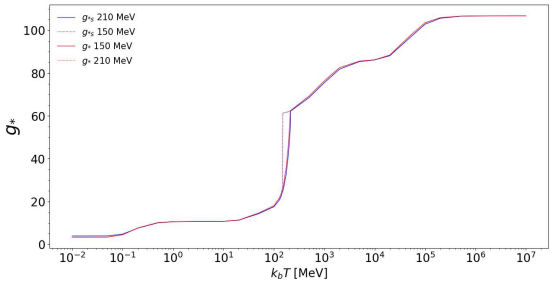

Figure A.1: Degrees of freedom as a function of temperature: g_* and g_{*s} are very similar. The dotted lines indicate the transition phase at 210 MeV, while the solid lines correspond to 150 MeV. Note that as you read the plot from left to right, the temperature increases, which means you are moving backward in time.

can see that g_* and g_{*s} are characterized by two distinct epochs. The first epoch is when there is no entropy production and each particle species contributing to the total energy and entropy densities can be considered as an ideal gas. The second phase begins with the QCD transition, occurring at $T \simeq 150 - 300$ MeV, during which these approximations are no longer valid. In this transition phase, gluons and all quarks are no longer free but are confined within hadrons, leading to an abrupt reduction in the number of degrees of freedom (the QCD transition phase marks this change).
We note that we have frequently used the conservation of entropy per comoving volume, which is not as valid during the QCD phase transition.

Bibliography

For the evidences for Dark Matter and the empirical facts about it:

- D. Hopper, *TASI 2008 Lectures on Dark Matter*, arXiv:0901.4090
- D.Hopper, G. Bertone, *A History of Dark Matter*, arXiv:1605.04909,
- G.B. Gelmini, TASI 2014 Lectures: *The Hunt for Dark Matter*, arXiv:1502.01320
- M. Lisanti, *Lectures on Dark Matter Physics*, arXiv:1603.03797

For the Boltzmann equation and freeze-out:

- E.W. Kolb and M.S. Turner, *The Early Universe.* Addison-Wesley Publishing Company,1989.
- D. Hopper, *TASI 2008 Lectures on Dark Matter*, arXiv:0901.4090
- G.B. Gelmini, TASI 2014 Lectures: *The Hunt for Dark Matter*, arXiv:1502.01320

For the thermal average section:

- P.Gondolo, G.B. Gelmini *Cosmic abundances of stable particles: improved analysis* , Nuc. Phys. B360 (1991) 145-179
- M. E. Peskin, D. V. Schroeder, *An Introduction To Quantum Field Theory*, Frontiers in Physics. Westview Press, 1995

For the number degrees of freedom in the early universe:

- P.Gondolo, G.B. Gelmini *Cosmic abundances of stable particles: improved analysis* , Nuc. Phys. B360 (1991) 145-179
- L. Husdal *On Effective Degrees of Freedom in the Early Universe*, arXiv:1609.04979

For the thermal average near a resonance:

- K.Griest, D.Seckel, *Three exceptions in the calculation of relic abundances*, Phys. Rev.B43 (1991) 3191-3203
- P.Gondolo, G.B. Gelmini *Cosmic abundances of stable particles: improved analysis* , Nuc. Phys. B360 (1991) 145-179

For the cosmology part:

- E.W. Kolb and M.S. Turner, *The Early Universe.* Addison-Wesley Publishing Company,1989.
- A. Liddle, *An Introduction to Modern Cosmology.* Wiley, 2015.
- S. M. Carroll, *Spacetime and geometry: an introduction to General Relativity* Cambridge University Press, 2019.